Geophysical Research Letters

RESEARCH LETTER
10.1029/2019GL083035

Key Points:
- Continental margin sediments off northwestern Australia record large continental aridity shifts at 5.3, 3.8, 2.8, and 1.4 Ma
- Grain size and chemistry of the terrigenous fraction of seafloor sediments and source areas on land allow a characterization of river mud
- Monsoonal activity responds to changes in Indian-Ocean SSTs and drives river runoff in northwestern Australia

Supporting Information:
- Supporting Information S1
- Figure S1
- Figure S2
- Figure S3
- Figure S4
- Figure S5
- Figure S6
- Figure S7
- Figure S8
- Figure S9
- Figure S10
- Figure S11
- Figure S12

Correspondence to:
J.-B. W. Stuut,
jbstuut@nioz.nl

Citation:
Stuut, J.-B. W., De Deckker, P., Saavedra-Pellitero, M., Bassinot, F., Drury, A. J., Walczak, M. H., et al. (2019). A 5.3-million-year history of monsoonal precipitation in northwestern Australia. *Geophysical Research Letters*, *46*, 6946–6954. https://doi.org/10.1029/2019GL083035

Received 29 MAR 2019
Accepted 5 JUN 2019
Accepted article online 10 JUN 2019
Published online 28 JUN 2019

©2019. American Geophysical Union.
All Rights Reserved.

A 5.3-Million-Year History of Monsoonal Precipitation in Northwestern Australia

Jan-Berend W. Stuut[1,2,3], Patrick De Deckker[4], Mariem Saavedra-Pellitero[5,6], Franck Bassinot[7], Anna Joy Drury[2], Maureen H. Walczak[4], Kana Nagashima[8], and Masafumi Murayama[9]

[1]NIOZ-Royal Netherlands Institute for Sea Research and Utrecht University, Texel, The Netherlands, [2]MARUM-Center for Marine Environmental Sciences, Bremen University, Bremen, Germany, [3]Department of Earth Sciences, Faculty of Science, Vrije Universiteit Amsterdam, Amsterdam, The Netherlands, [4]Research School of Earth Sciences, Australian National University, Canberra, ACT, Australia, [5]Department of Geosciences, Bremen University, Bremen, Germany, [6]Now at School of Geography, Earth and Environmental Sciences, University of Birmingham, Birmingham, UK, [7]LSCE-Laboratoire des Sciences du Climate et de l'Environnement (CEA, CNRS, UVSQ), Gif-sur-Yvette, France, [8]Research Institute for Global Change, Japan Agency for Marine-Earth Science and Technology, Yokosuka, Japan, [9]Center for Advanced Marine Core Research, Kochi University, Kochi, Japan

Abstract New proxy records from deep-sea sediment cores from the northwestern continental margin of Western Australian reveal a 5.3 million year (Ma) history of aridity and tropical monsoon activity in northwestern Australia. Following the warm and dry early Pliocene (~5.3 Ma), the northwestern Australian continent experienced a gradual increase in humidity peaking at about 3.8 Ma with higher than present-day rainfall. Between 3.8 and about 2.8 Ma, climate became progressively more arid with more rainfall variability. Coinciding with the onset of the Northern Hemisphere glaciations and the intensification of the Northern Hemisphere monsoon, aridity continued to increase overall from 2.8 Ma until today, with greater variance in precipitation and an increased frequency of large rainfall events. We associate the observed large-scale fluctuations in Australian aridity with variations in Indian Ocean sea surface temperatures, which largely control the monsoonal precipitation in northwestern Australia.

Plain Language Summary Australia is the driest inhabited continent on the planet, with its moisture mostly sourced from the tropical monsoon in the north and the southern westerlies in the south. The continent has experienced large climate fluctuations in the geologic past, but long continuous records of paleoenvironmental changes are lacking, particularly prior to ~0.55 Ma. Here, we address this paucity by presenting a continuous and fluctuating record of continental aridity and monsoonal activity in northwestern Australia since the Pliocene (5.3 Ma). These records are based on bulk-chemical X-Ray Fluorescence scans and particle-size distributions of the terrigenous fraction in two marine sediment cores from the NW Western Australian continental margin. A comparison with present-day sources of windblown and fluvial sediments taken near the NW Western Australian coast corroborates our interpretation of the terrigenous fraction in the marine sediment cores. We show how the northwestern part of the Australian continent has experienced large climate fluctuations since 5.3 Ma, expressed by large aridity contrasts and great changes in monsoonal precipitation that are driven by Indian Ocean sea-surface temperatures.

1. Introduction

Present-day climate in NW Western Australia is characterized by dry winters and hot wet summers, typified by cyclones and cyclonic depressions of the Australian summer monsoon (Australian Bureau of Meteorology, 2017). Tropical cyclones develop during periods of high (higher than 26.5 °C; De Deckker, 2016; De Deckker et al., 2002; Tory & Dare, 2015) sea-surface temperatures (SSTs) in the Indian Ocean and Indo-Pacific Warm Pool (IPWP). Next to tropical cyclones, monsoonal precipitation is also brought about by so-called cyclonic depressions, which also deliver extensive amounts of rainfall. The strong seasonal contrast in precipitation causes major rivers to remain dry for most of the year and only discharge large floods, full of sediments, during the rainy season and mostly coinciding with cyclones and cyclonic depressions. The strong seasonality also results in large wind-driven dust outbreaks, which mostly occur in late spring-early summer prior to the rainy season when river/lake beds, and soils are driest (DustWatch Australia: Community-based wind erosion monitoring, 2017). Reflecting these seasonally contrasting

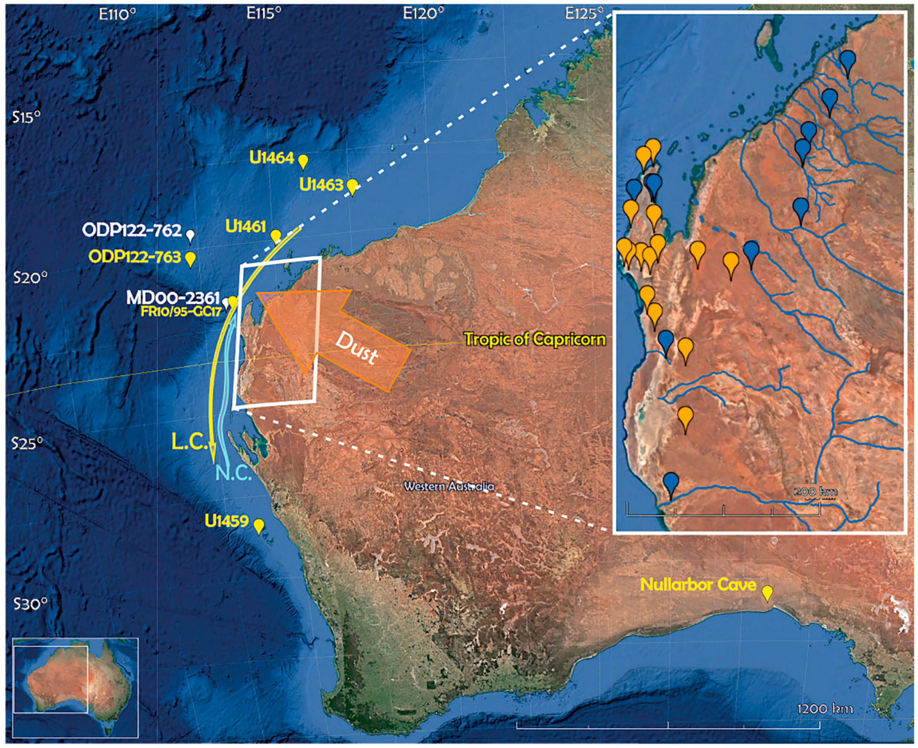

Figure 1. Google Earth map of northwestern Western Australia and its continental margin showing the positions of the two studied sites (ODP122-762B and MD00-2361 white pins), as well as—right insert—the land samples of river beds (blue pins) and dune systems (orange pins), for which the bulk chemical compositions are compared to those measured in the sediment cores (see supporting information). The large rivers draining into the eastern Indian Ocean are also shown. L.C. = Leeuwin Current; N.C. = Ningaloo (counter) Current. Cores of comparable studies are indicated with yellow pins: FR10/95-GC17 (van der Kaars & De Deckker, 2002; just east of MD00-2361), ODP122-763 (O'Brien et al., 2014); IODP356-U1464 (Groeneveld et al., 2017), IODP356-U1463 (Christensen et al., 2017), IODP356-U1461 (Ishiwa et al., 2019), IODP356-U1459 (Groeneveld et al., 2017) and Nullarbor Caves (Sniderman et al., 2016).

processes, the terrigenous sediment fraction that ends up on the northwestern Western Australian continental shelf and slope is a mixture of airborne dust emitted during the dry season and river-transported mud during the rainy season and in particular during monsoonal activity, some of which caused by cyclones (Stuut et al., 2014). There are many studies showing that fine-grained sediments supplied by rivers can travel long distances in the ocean before settling on the seafloor (Hopkins et al., 2013; Palma & Matano, 2017; Prins et al., 2000; Shanmugam, 2018; see supporting information).

Changes in environmental conditions in northwestern Western Australia are now well documented for the late Quaternary (last ~550 ka), notably indicating dryer (arid) conditions during glacials. Fossil pollen and charcoal in marine sediments from an adjacent core [van der Kaars & De Deckker, 2002; FR10/95-GC17; see Figure 1] located on the fringe of the IPWP reveal a much drier Last Glacial Maximum (LGM), characterized by a shrubland vegetation type as opposed to open *Eucalyptus* woodlands, which prevailed during the wetter period before the LGM (van der Kaars & De Deckker, 2002). Similarly, van der Kaars et al. (2006) demonstrated—based on pollen transfer functions applied to core top sediments—that the LGM was much drier than present, and several authors also found that the Australian-Indonesian monsoon did not operate at that time (Brown et al., 2009; Marshall & Lynch, 2008; Tripati et al., 2014; van der Kaars et al., 2006). These observations were mechanistically corroborated by a study offshore northwestern Western Australia of SSTs covering the past 550 ka, showing a 6–9 °C temperature drop during glacials (Spooner et al., 2011). Nevertheless, such a large SST reduction only occurred at the edge of the IPWP (where the studied core was obtained), whereas inside the IPWP, in the Timor Sea, SST dropped at the LGM by 4.2 ± 0.34 °C (Levi et al., 2007) and by 3.5 ± 0.48 °C in an adjacent core (Xu et al., 2008). Such a temperature drop from the modern value of 28.6 °C (De Deckker, 2016) would explain the drastic decline of monsoonal activity during glacial periods as a result of the reduction of convective cloud formation as seen today for the tropical Pacific Ocean when temperature is below 26 °C (Waliser & Graham, 1993), thereby decreasing heavy rainfall and monsoonal activity. In addition, there is evidence also that the intertropical convergence zone shifted northward from Australia during the LGM as demonstrated by Spooner et al. (2005) from a core in the Banda Sea. We can assume that this phenomenon was a repetition of previous glacial periods.

Based on particle-size distributions and major element geochemistry of marine sediments, Stuut et al. (2014) reconstructed paleoenvironmental conditions in northwestern Western Australia for the last 550 ka. Generally, this record describes a glacial-interglacial variability between colder and drier glacials characterized by coarse-grained dust input versus warm and humid interglacials characterized by increased river runoff. In particular, the fluvially transported sediments, principally engendered by monsoonal rains, dominate the sedimentary record with thick sequences of brown muds mixed with pelagic sediments. During dry phases, the sediment is beige in color and contains ample quartz grains and other minerals that are blown offshore (Stuut et al., 2014). Ishiwa et al. (2019), based on X-Ray Fluorescence (XRF) records of nearby site U1461, derive a drying trend throughout the last 14,000 years. Further continuous records of Australia's hydroclimate are scarce, particularly in the northwestern part of the continent [see Christensen et al., 2017, for a compilation of Neogene climate records]. Christensen et al. (2017) present a record of downhole measurements at IODP site U1463 (see Figure 1 for location) in which they interpret the natural gamma radiation in the sediments as a measure for the concentration of the elements K, Th, and U, which are interpreted as reflecting windblown or riverine flux of detrital material in the marine system. Both U(%) and Th/K are interpreted as proxies for aridity, whereas K(%) is interpreted as a proxy for humidity and continental runoff and terrigenous input. Subsequently, they speculate that the observed variations in windblown or riverine fluxes are driven by the Indonesian Throughflow, with a large shift from dry to wet conditions during the Miocene-Pliocene transition and a general drying trend between 3.4 and 1 Ma. The upper 72 m of the U1463 core record, spanning the upper 1 Ma, has not been measured in this core. During the same IODP leg, site U1459 was drilled at 28°4′S/113°3E (see Figure 1 for location) and also measured with the same gamma ray scanner, resulting in paleoclimate records for most of the Miocene [18–6 Ma; Groeneveld et al., 2017]. Groeneveld et al. (2017) interpret their derived K(%) as showing variations in riverine input and, thus, the amount of rainfall over southwest Western Australia. As opposed to the northern Australian record, they derive a very dry Early and Middle Miocene and a gradual wetting trend toward the Pliocene, which they ascribe to an equatorward migration of the southern westerlies. In contrast, and although being related to the same moisture source, on the basis of fossil pollen in cave deposits in southern Australia (see Figure 1 for location), Sniderman et al. (2016) derive a Southern Hemisphere hydroclimate record from the latest Miocene to the middle Pliocene, showing an abrupt onset of warm and wet climates early within the Pliocene.

Here, we present new XRF data from the lower part of core (MD00-2361), extending the record down to 1 Ma (Figure 2). We additionally present new data from a neighboring sediment core ODP122-762 (260 km away and some ~350 km away from the nearest present-day Australian coastline; see Figure 1) which provides a nearly identical climate record to MD00-2361 for the last 1 Ma and extends the environmental reconstructions down to the Miocene-Pliocene boundary (5.3 Ma). To study the aeolian and fluvial end members, we also conducted a field study in the source areas of the sediment cores (viz. northwestern Western Australia bordering the coastline; Figure 1). We sampled both river beds and sand dunes, for which we then analyzed the bulk chemical composition in the same way as we did for the marine sediment cores (see supporting information).

On the basis of their combined particle-size and chemical analyses of the upper 500 ka of core MD00-2361, Stuut et al. (2014) argued that the Fe/Ca ratio reflects the relative contributions of terrigenous and marine fractions in the core. Interglacial stages are characterized by huge amounts of river runoff, resulting in thick brown mud deposits (see Stuut et al., 2014, their Figure 2), as opposed to layers of carbonate-rich hemipelagic sediments deposited during glacial stages. In addition, these glacial stages are also characterized by coarse-grained windblown quartz particles and other robust mineral grains that only rarely occur during interglacial stages, which is reflected in the Zr/Fe ratio.

2. Material and Methods

Site ODP122-762 hole B (19°53.24′S, 112°15.24′E, 1,360-m water depth; Figure 1) was drilled on the top of the Montebello Saddle, which forms a large plateau on the northwestern Australian continental slope

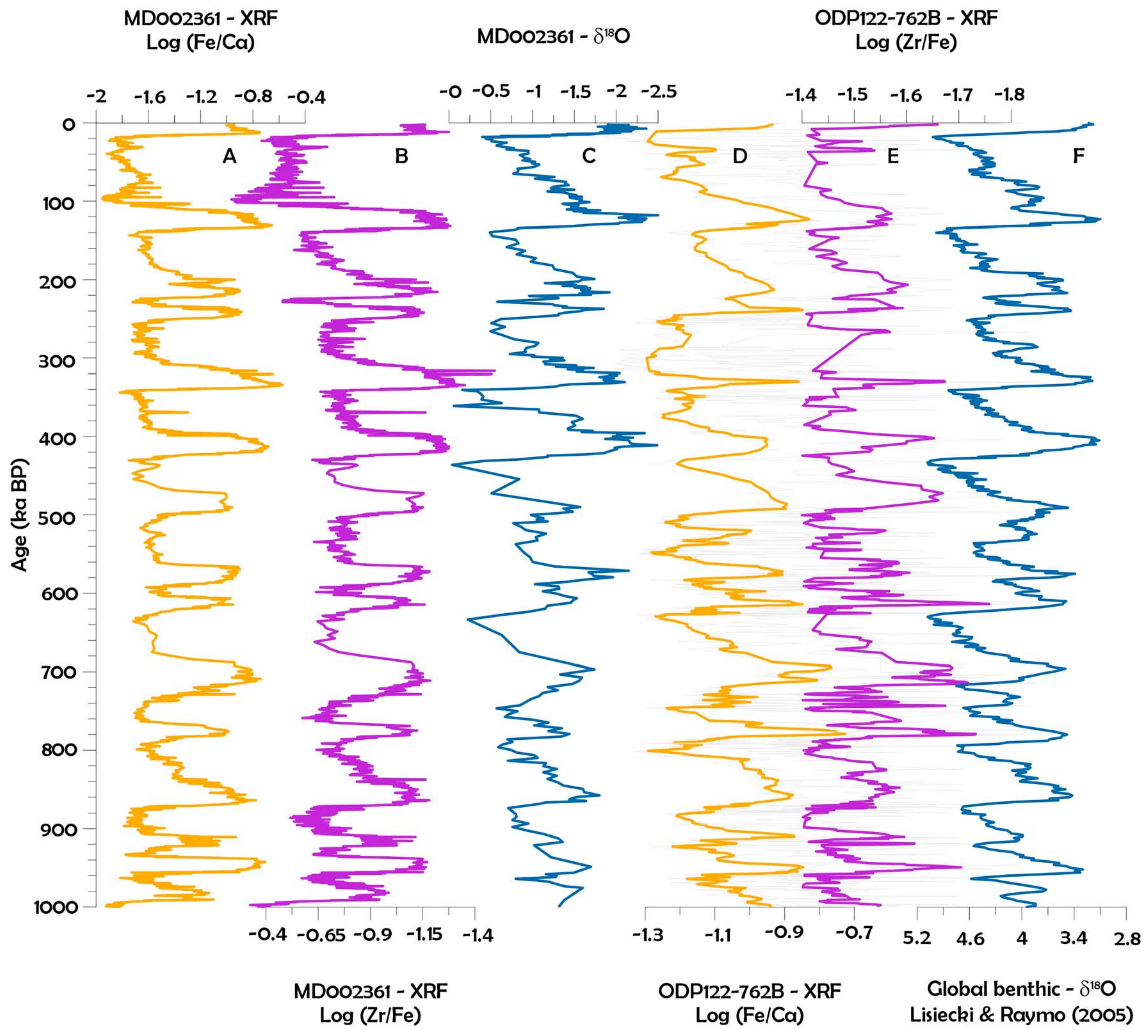

Figure 2. Proxy records for northwestern Western Australian climate of the last 1 Ma. (A) MD00-2361 Log Fe/Ca, a proxy for the amount terrigenous sediments (both aeolian dust and fluvial mud). (B) MD00-2361 Log Zr/Fe (note reversed axis), a proxy for the proportion river mud versus aeolian-dust input. (C) MD00-2361 $\delta^{18}O$, measured on *Globigerinoides ruber*, following Spooner et al. (2011), reflecting the convolved influences of global sea level and local temperature/salinity fluctuations. The lower 450 ka of the MD00-2361 records are new data, complementary to Stuut et al. (2014). (D) ODP122-762B Log Fe/Ca raw data in gray, 5-point running average in orange. (E) ODP122-762B Log Zr/Fe (note reversed axis), raw data in gray, five-point running average in purple. (F) Published $\delta^{18}O$ record of the global oxygen-isotope stack (Lisiecki & Raymo, 2005).

(Haq et al., 1990). The age model was constructed using initially the existing preliminary shipboard magnetostratigraphy (Tang, 1992), which was slightly revised and complemented by new calcareous nannofossil datum events based on Anthonissen and Ogg (2012), which resulted in 16 additional tie points (Table S1). Subsequently, a visual correlation of the Log (Fe/Ca) XRF record and the Lisiecki and Raymo (2005) $\delta^{18}O$ stack curve was made, which resulted in 175 additional tie points (Figure S7, available at the www.pangaea.de data archive web site).

Core MD00-2361 (22°04.92′S, 113°28.63′E, 1,805-m water depth; Figure 1) was retrieved from a saddle in between the Cape Range Canyon and the Cloates Canyon, to avoid mass deposits that may have travelled through these canyons (Spooner et al., 2011). The age model of the upper 550 ka of the core was published by Spooner et al. (2011) based on the $\delta^{18}O$ of *Globigerinoides ruber*. Following their method, for this study, we increased the resolution below ~250 ka and additionally extended it to 1 Ma.

Bulk chemical (XRF) data were obtained at 2-cm resolution for core ODP122-762B at the Kochi Core Center, Japan, using an ITRAX core scanner and for core MD00-2361 at NIOZ, the Netherlands (see supporting information for details). Following Stuut et al. (2014), the Log (Fe/Ca) is used as a proxy for land-derived material and Log (Zr/Fe) as a proxy for the contribution of fluvial mud versus aeolian dust. Bulk chemical

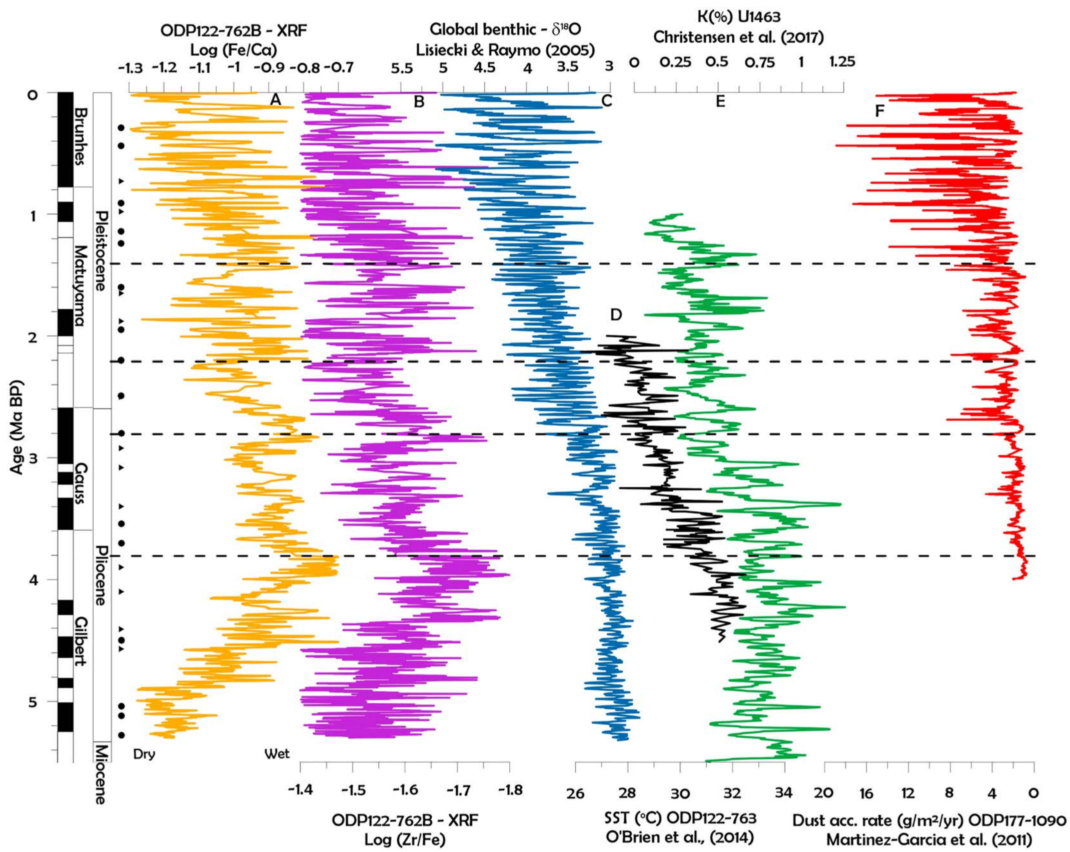

Figure 3. Proxy records for northwestern Australian climate of the last 5.3 Ma. Black dots ($N = 16$) on the left show new tie points provided by calcareous nannofossil-based biostratigraphy (black triangles, $N = 13$; see Table S1), which served as initial age model, together with the published shipboard magnetostratigraphic tie points (Tang, 1992). This initial age model was then refined by additional tie points ($N = 175$) after visual correlation with the L&R2005 stack (Lisiecki & Raymo, 2005). (A) Log (Fe/Ca, five-point running average in orange), (B) Log (Zr/Fe, five-point running average in purple; note the reversed axis to facilitate visibility/correlation) are used as proxies for terrigenous-sediment input and proportion river mud versus aeolian-dust deposition, respectively. (C) The oxygen isotope record (Lisiecki & Raymo, 2005; blue) represents global sea level combined with other factors such as oceanic temperatures as evidenced by the difference in amplitude between the start and end of the Pliocene. (D) SST in ODP122-763A [O'Brien et al., 2014; black; see Figure 1 for location], (E) K (%) in U1463 [Christensen et al., 2017; green; see Figure 1 for location], and (F) Dust in ODP-177-190 (Martinez-Garcia et al., 2011; red) and are shown for comparison. SST = sea surface temperature.

(XRF, Avaatech at NIOZ) data were also obtained on discrete samples from river beds and dunes in the source area of the sediments that are blown and flown to the core sites (Figures 1 and S6).

3. Results

The bulk chemical records of the two analyzed cores show nearly identical patterns for the last 1 Ma, characterized by large-amplitude changes in both Zr/Fe and Fe/Ca (Figure 2). Cycles in Zr/Fe and Fe/Ca also line up with the planktonic $\delta^{18}O$ record of Spooner et al. (2011) indicating a consistent relationship between glacial/interglacial conditions and northwestern Western Australian climate over the last 1 Ma. Core ODP122-762 contains a detailed and continuous Pliocene-Pleistocene paleoclimate archive of continental northwestern Australia (Figure 3). It shows a gradual increase in precipitation from 5.3 to 3.8 Ma and a more rapid return to drier conditions from 3.8 Ma to the present on which two types of variations are superimposed: (1) long-term oscillations (>500 ka) and (2) orbital-scale (41 and 100 ka) glacial cyclicity. From 2.8 to 2.2 Ma, the marine sediments show a decreasing trend in the terrigenous sediment component. A transitional period with dramatic high-amplitude variability in discharges occurred between 2.2 and 1.4 Ma. Between 1.4 Ma and the present, the sediments gradually became dominated by marine pelagic carbonates once more and the amplitude of changes between dry and wet intervals increased dramatically.

From the observation that the glacial-interglacial succession continues throughout the last 1 Ma in both cores as well as during the past 5.3 Ma in the ODP core, we conclude that our proxy records from

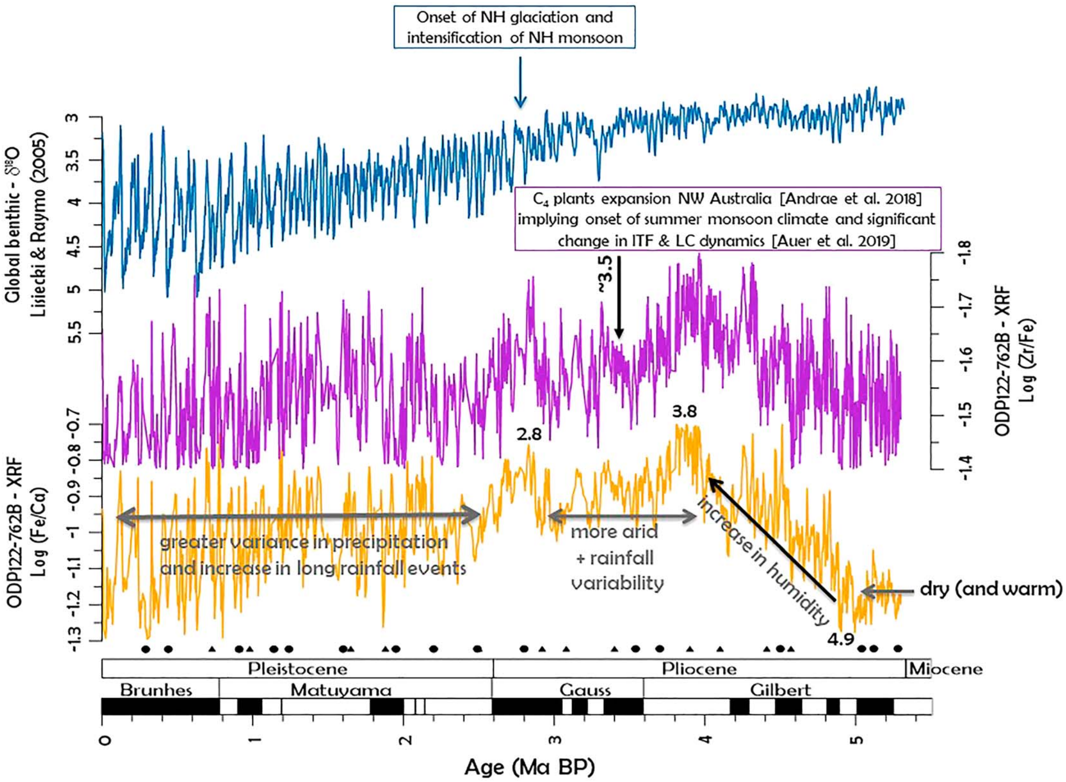

Figure 4. Proxy records for northwestern Australian climate of the past 5.3 Ma (refer to Figure 3 for more details) obtained from ODP122-762B. The main trends interpreted from our records are shown, in comparison with the global benthic $\delta^{18}O$ stack (Lisiecki & Raymo, 2005). The major shift in C_4 plants implying onset of summer monsoon climate in Australia at ~3.5 Ma, as described by Andrae et al. (2018), and the reorganization of the ITF and LC north of Australia by Auer et al. (2019) due to tectonic changes are also shown. See text for further discussion on the chronology of such change.

northwestern Western Australia provide a regional signal of precipitation through river-sediment discharge and deposition at sea.

4. Discussion

Modern precipitation around the IPWP and adjacent regions, including northwestern Australia, is dictated by the summer monsoon of which about 70% of the rainfall is caused by the occurrence of tropical cyclones (Dare et al., 2012). We therefore interpret the chemical records of our sediment cores in terms of runoff related to monsoonal rains in northwestern Australia as it is predominantly when cyclonic depressions transgress over northern Australia that huge fluvial discharges occur at sea (Figure S2).

Since the beginning of the Pliocene at 5.3 Ma, global temperatures were substantially higher than they are today (Fedorov et al., 2006) with likely significantly higher occurrence of monsoonal rains and even possibly tropical cyclones (Fedorov et al., 2010), which helped maintain enduring El Niño conditions and which is also reflected in our records (Figure 4). See also Wara et al. (2005), who refer to it as "a permanent El Niño." This contrasts with the present day, when monsoonal precipitation is most intense during neutral and La Niña years (Dare, 2013), related to the increased zonal SST and SSS gradients in the tropical Pacific Ocean (see supporting information). We hypothesize that this was also the case during the mid-Pliocene as our records show a decrease in runoff at 3.8 Ma.

In addition, Andrae et al. (2018) in their pollen studies on core ODP 763A reveal the onset of Australian C_4-plant expansion at ~3.5 Ma (Figure 4). This timing coincides almost exactly with inferred changes in the Indonesian Throughflow and Leeuwin-Current dynamics recognized in core U1463 by Auer et al. (2019). Our records show a much earlier shift in the elemental ratio records after 3.8 Ma. We note that Auer et al.'s (2019) record does not extend that far back in time. In addition, Andrae et al.'s (2018) record for the percentage of C_4 plants has only one analysis between ~3.5 and ~4.2 Ma. It may be therefore that the humid phase in Andrea et al.'s (2018) Figure 3d could have ended earlier than 3.5 Ma.

From about 3 Ma onward, due to global cooling and the increasing latitudinal temperature gradients since the Pliocene, there was an amplification of obliquity cycles in equatorial SSTs (Fedorov et al., 2006) and a gradual drying up of the northwestern Australian continent. A suite of additional processes has been suggested as possible drivers of the ongoing global cooling during the Pliocene, including lower global sea level (Gallagher et al., 2001), closing of the Panama Seaway (Karas et al., 2017), uplift of the Tibetan Plateau (An et al., 2001), and northward movement of the Australian continent, possibly partially blocking the Indonesian Throughflow (Cane & Molnar, 2001) and tectonic readjustment, as discussed by Auer et al. (2019). Eventually, all these changes led to glaciation of the Northern Hemisphere. Soon after, our records show a greater variance in precipitation and an increase in long rainfall events (Figure 4).

Modeling experiments have suggested that reducing the warm water exchange between the Pacific and Indian Oceans via the Indonesian Throughflow may have led to a precipitation dipole, with increased rainfall over eastern Australia and up to 30% reduction of rainfall over northwestern Australia (Krebs et al., 2011). The gradual drying trend is clearly reflected in our records, as well as increasing amplitude changes between wet and dry phases since about 2.4 Ma, similar to increased amplitudes in the global benthic $\delta^{18}O$ stack (Lisiecki & Raymo, 2005; Figure 3C) as well as the Southern Hemisphere dust fluxes reconstructed from a sediment core from the South Atlantic (Martinez-Garcia et al., 2011; Figure 3F). At the same time, our Log (Fe/Ca) record shows a general decrease since 1.4 Ma, which we interpret as a gradual decrease in river runoff, which is paralleled by an increase in dust fluxes in the Atlantic Ocean.

Our records do not show a clear relation with the recently published K(%) record, interpreted as proxy for continental aridity, measured in IODP core U1463 [Christensen et al., 2017; see Figure 1 for location and Figure 3E for the K(%) record], which could be related to the large smoothing that occurs during downhole natural gamma ray measurements. However, both records show a similar high-amplitude signal during both the Late Miocene and the Pliocene, which is not apparent in the benthic $\delta^{18}O$ stack and which we interpret as a sensitive response to changes in the driving mechanism. Comparison of our records to the SST record of nearby core ODP122-763A [Karas et al., 2011; revised by O'Brien et al., 2014] does not show an obvious correlation, apart from a decreasing temperature trend throughout the Pliocene. However, particularly for the earlier part of the record (4.4–3.6 Ma), when our records indicate wettest conditions on the northwestern Australian continent, the SSTs are above 30.5 °C, therefore implying that high rainfall can be generated despite the fact that convective clouds are absent above that threshold today (Waliser & Graham, 1993).

Finally, the Late Pleistocene part of our record shows a strong resemblance to the global $\delta^{18}O$ stack (Lisiecki & Raymo, 2005), including a shift from obliquity (41 ka)-dominated cyclicity to eccentricity (100 Ka)-dominated climate swings since about the mid-Pleistocene transition at about 800 ka (Lisiecki, 2010; see supporting information for time series analysis).

5. Conclusions

Our study suggests that the Australian continent has experienced a vivid environmental history with large fluctuations in monsoonal activity and very likely caused by monsoonal rainfall. This has important implications for the evolution of the fauna and flora as well as the development of the fire-adapted vegetation (Martin, 2006; Miller et al., 2005). Although northwestern Australia has become increasingly arid since the mid-Pliocene (~3.8 Ma), our records suggest the Holocene exists in the wettest phase of the high-frequency, large-amplitude swings in discharge states that have characterized regional climate variability since the early Pleistocene (~2.2 Ma) with rainfall rates among the highest of the past 5.3 Ma.

Acknowledgments
We thank Lallan Gupta and his team at KCC/JAMSTEC for their help with all the ODP core sections. We thank both Rineke Gieles (NIOZ) and Yagyu Shinsuke (KCC/JAMSTEC) for assistance with XRF core scanning. J. B. W. S. acknowledges funding from the Japanese Society for the Promotion of Science (JSPS Grant S16116). This study was performed under the cooperative research program of Center for Advanced Marine Core Research (CMCR), Kochi University 16B050. We are grateful to the Editor Valerie Trouet, for her efforts to have our manuscript reviewed and acknowledge the reviewers L. Lisiecki and an anonymous reviewer. All data presented in this manuscript are available in PANGAEA (www.pangaea.de). This is LSCE contribution 6649.

References

An, Z., Kutzbach, J. E., Prell, W. L., & Porter, S. C. (2001). Evolution of Asian monsoons and phased uplift of the Himalaya-Tibetan plateau since Late Miocene times. *Nature*, *411*(6833), 62–66.

Andrae, J. W., McInerney, F. A., Polissar, P. J., Sniderman, J. M. K., Howard, S., Hall, P. A., & Phelps, S. R. (2018). Initial expansion of C4 vegetation in Australia during the Late Pliocene. *Geophysical Research Letters*, *45*, 4831–4840. https://doi.org/10.1029/2018GL077833

Anthonissen, D. E., & Ogg, J. G. (2012). Appendix 3—Cenozoic and Cretaceous biochronology of planktonic foraminifera and calcareous nannofossils. In *The Geologic Time Scale*, edited, (pp. 1083–1127). Boston: Elsevier. https://doi.org/10.1016/B978-0-444-59425-9.15003-6

Auer, G., de Vleeschouwer, D., Smith, R. A., Bogus, K., Groeneveld, J., Grunert, P., et al. (2019). Timing and pacing of Indonesian Throughflow restriction and its connection to late Pliocene climate shifts. *Paleoceanography and Paleoclimatology*, *34*, 635–657. https://doi.org/10.1029/2018PA003512

Australian Bureau of Meteorology (2017), Climate data online, edited, Australian Government.

Brown, J., Lynch, A. H., & Marshall, A. G. (2009). Variability of the Indian Ocean Dipole in coupled model paleoclimate simulations. *Journal of Geophysical Research*, *114*, D11105,. https://doi.org/10.1029/2008JD010346

Cane, M. A., & Molnar, P. (2001). Closing of the Indonesian seaway as a precursor to east African aridification around 3-4[thinsp]million years ago. *Nature*, *411*(6834), 157–162. https://doi.org/10.1038/35075500

Christensen, B. A., Renema, W., Henderiks, J., de Vleeschouwer, D., Groeneveld, J., Castañeda, I. S., et al., & IODP Expedition 356 Scientists (2017). Indonesian Throughflow drove Australian climate from humid Pliocene to arid Pleistocene. *Geophysical Research Letters*, *44*, 6914–6925. https://doi.org/10.1002/2017GL072977

Dare, R. A. (2013). Seasonal tropical cyclone rain volumes over Australia. *Journal of Climate*, *26*(16), 5958–5964. https://doi.org/10.1175/JCLI-D-12-00778.1

Dare, R. A., Davidson, N. E., & McBride, J. L. (2012). Tropical cyclone contribution to rainfall over Australia. *Monthly Weather Review*, *140*(11), 3606–3619. https://doi.org/10.1175/MWR-D-11-00340.1

De Deckker, P. (2016). The Indo-Pacific Warm Pool: Critical to world oceanography and world climate. *Geoscience Letters*, *3*(1). https://doi.org/10.1186/s40562-016-0054-3

De Deckker, P., Tapper, N. J., & van der Kaars, S. (2002). The status of the Indo-Pacific Warm Pool and adjacent land at the Last Glacial Maximum. *Global and Planetary Change*, *35*(1–2), 25–35.

DustWatch Australia: Community-based wind erosion monitoring (2017), An interactive map of dust occurrences throughout the Australian continent, edited.

Fedorov, A. V., Brierley, C. M., & Emanuel, K. (2010). Tropical cyclones and permanent El Niño in the early Pliocene epoch. *Nature*, *463*(7284), 1066–1070. https://doi.org/10.1038/nature08831

Fedorov, A. V., Dekens, P. S., McCarthy, M., Ravelo, A. C., deMenocal, P. B., Barreiro, M., et al. (2006). The Pliocene paradox (Mechanisms for a Permanent El Niño). *Science*, *312*(5779), 1485–1489. https://doi.org/10.1126/science.1122666

Gallagher, S. J., Smith, A. J., Jonasson, K., Wallace, M. W., Holdgate, G. R., Daniels, J., & Taylor, D. (2001). The Miocene palaeoenvironmental and palaeoceanographic evolution of the Gippsland Basin, Southeast Australia: A record of Southern Ocean change. *Palaeogeography, Palaeoclimatology, Palaeoecology*, *172*(1–2), 53–80. https://doi.org/10.1016/S0031-0182(01)00271-1

Groeneveld, J., Henderiks, J., Renema, W., McHugh, C. M., de Vleeschouwer, D., Christensen, B. A., et al., & Expedition 356 Scientists (2017). Australian shelf sediments reveal shifts in Miocene Southern Hemisphere westerlies. *Science Advances*, *3*(5), e1602567. https://doi.org/10.1126/sciadv.1602567

Haq, B. U., von Rad, U., O'Connell, S., & expedition 122 scientists (1990). *Summary and highlights of Leg 122, Affiliation (analytic)*, (Vol. 122, p. 5). Washington, DC: Natl. Sci. Found., Mar. Geol. and Geophys.

Hopkins, J., Lucas, M., Dufau, C., Sutton, M., Stum, J., Lauret, O., & Channelliere, C. (2013). Detection and variability of the Congo River plume from satellite derived sea surface temperature, salinity, ocean colour and sea level. *Remote Sensing of Environment*, *139*, 365–385. https://doi.org/10.1016/j.rse.2013.08.015

Ishiwa, T., Yokoyama, Y., Reuning, L., McHugh, C. M., De Vleeschouwer, D., Gallagher, S. J., & Science, P. (2019). Australian Summer Monsoon variability in the past 14,000 years revealed by IODP Expedition 356 sediments. *Progress in Earth and Planetary Science*, *6*(1). https://doi.org/10.1186/s40645-019-0262-5

Karas, C., Nürnberg, D., Bahr, A., Groeneveld, J., Herrle, J. O., Tiedemann, R., & deMenocal, P. B. (2017). Pliocene oceanic seaways and global climate. *Scientific Reports*, *7*(1), 39842. https://doi.org/10.1038/srep39842

Karas, C., Nürnberg, D., Tiedemann, R., & Garbe-Schönberg, D. (2011). Pliocene Indonesian Throughflow and Leeuwin Current dynamics: Implications for Indian Ocean polar heat flux. *Paleoceanography*, *26*, PA2217. https://doi.org/10.1029/2010PA001949

Krebs, U., Park, W., & Schneider, B. (2011). Pliocene aridification of Australia caused by tectonically induced weakening of the Indonesian throughflow. *Palaeogeography, Palaeoclimatology, Palaeoecology*, *309*(1–2), 111–117. https://doi.org/10.1016/j.palaeo.2011.06.002

Levi, C., Labeyrie, L., Bassinot, F., Guichard, F., Cortijo, E., Waelbroeck, C., et al. (2007). Low-latitude hydrological cycle and rapid climate changes during the last deglaciation. *Geochemistry, Geophysics, Geosystems*, *8*, Q05N12. https://doi.org/10.1029/2006GC001514

Lisiecki, L. E. (2010). Links between eccentricity forcing and the 100,000-year glacial cycle. *Nature Geoscience*, *3*(5), 349–352. https://doi.org/10.1038/ngeo828

Lisiecki, L. E., & Raymo, M. E. (2005). A Pliocene-Pleistocene stack of 57 globally distributed benthic $\delta^{18}O$ records. *Paleoceanography*, *20*, PA1003. https://doi.org/10.1029/2004PA001071

Marshall, A. G., & Lynch, A. H. (2008). The sensitivity of the Australian summer monsoon to climate forcing during the late Quaternary. *Journal of Geophysical Research*, *113*, D11107. https://doi.org/10.1029/2007JD008981

Martin, H. A. (2006). Cenozoic climatic change and the development of the arid vegetation in Australia. *Journal of Arid Environments*, *66*(3), 533–563. https://doi.org/10.1016/j.jaridenv.2006.01.009

Martinez-Garcia, A., Rosell-Mele, A., Jaccard, S. L., Geibert, W., Sigman, D. M., & Haug, G. H. (2011). Southern Ocean dust-climate coupling over the past four million years. *Nature*, *476*(7360), 312–315. https://doi.org/10.1038/nature10310

Miller, G. H., Fogel, M. L., Magee, J. W., Gagan, M. K., Clarke, S. J., & Johnson, B. J. (2005). Ecosystem collapse in Pleistocene Australia and a human role in megafaunal extinction. *Science*, *309*(5732), 287–290. https://doi.org/10.1126/science.1111288

O'Brien, C. L., Foster, G. L., Martínez-Botí, M. A., Abell, R., Rae, J. W. B., & Pancost, R. D. (2014). High sea surface temperatures in tropical warm pools during the Pliocene. *Nature Geoscience*, *7*(8), 606–611. https://doi.org/10.1038/ngeo2194

Palma, E. D., & Matano, R. P. (2017). An idealized study of near equatorial river plumes. *Journal of Geophysical Research: Oceans*, *122*, 3599–3620. https://doi.org/10.1002/2016JC012554

Prins, M. A., Postma, G., Cleveringa, J., Cramp, A., & Kenyon, N. H. (2000). Controls on terrigenous sediment supply to the Arabian Sea during the late Quaternary: The Indus Fan. *Marine Geology*, *169*(3-4), 327–349. https://doi.org/10.1016/S0025-3227(00)00086-4

Shanmugam, G. (2018). A global satellite survey of density plumes at river mouths and at other environments: Plume configurations, external controls, and implications for deep-water sedimentation. *Petroleum Exploration and Development*, *45*(4), 640–661. https://doi.org/10.1016/S1876-3804(18)30069-7

Sniderman, J. M. K., Woodhead, J. D., Hellstrom, J., Jordan, G. J., Drysdale, R. N., Tyler, J. J., & Porch, N. (2016). Pliocene reversal of late Neogene aridification. *Proceedings of the National Academy of Sciences*, *113*(8), 1999–2004. https://doi.org/10.1073/pnas.1520188113

Spooner, M. I., Barrows, T. T., De Deckker, P., & Paterne, M. (2005). Palaeoceanography of the Banda Sea, and Late Pleistocene initiation of the Northwest Monsoon. *Global and Planetary Change*, *49*(1-2), 28–46. https://doi.org/10.1016/j.gloplacha.2005.05.002

Spooner, M. I., De Deckker, P., Barrows, T. T., & Fifield, L. K. (2011). The behaviour of the Leeuwin Current offshore NW Australia during the last five glacial-interglacial cycles. *Global and Planetary Change*, *75*(3-4), 119–132. https://doi.org/10.1016/j.gloplacha.2010.10.015

Stuut, J.-B. W., Temmesfeld, F., & De Deckker, P. (2014). A 550 kyr record of aeolian activity near North West Cape, Australia: Inferences from grain-size distributions and bulk chemistry of SE Indian Ocean deep-sea sediments. *Quaternary Science Reviews*, *83*, 83–94. https://doi.org/10.1016/j.quascirev.2013.11.003

Tang, C. (1992). Paleomagnetism of Cenozoic sediments in Holes 762B and 763A, central Exmouth Plateau, Northwest Australia. In U. von Rad, B. U. Haq, et al. (Eds.), *Proceedings of the Ocean Drilling Program, Scientific Results*, (pp. 717–733). College Station, TX: Ocean Drilling Program.

Tory, K. J., & Dare, R. A. (2015). Sea surface temperature thresholds for tropical cyclone formation. *Journal of Climate*, *28*(20), 8171–8183. https://doi.org/10.1175/JCLI-D-14-00637.1

Tripati, A. K., Sahany, S., Pittman, D., Eagle, R. A., Neelin, J. D., Mitchell, J. L., & Beaufort, L. (2014). Modern and glacial tropical snowlines controlled by sea surface temperature and atmospheric mixing. *Nature Geoscience*, *7*(3), 205–209. https://doi.org/10.1038/ngeo2082

van der Kaars, S., & De Deckker, P. (2002). A Late Quaternary pollen record from deep-sea core Fr10/95, GC17 offshore Cape Range Peninsula, northwestern Western Australia. *Review of Palaeobotany and Palynology*, *120*(1–2), 17–39. https://doi.org/10.1016/S0034-6667(02)00075-1

van der Kaars, S., De Deckker, P., & Gingele, F. X. (2006). A 100 000-year record of annual and seasonal rainfall and temperature for northwestern Australia based on a pollen record obtained offshore. *Journal of Quaternary Science*, *21*(8), 879–889. https://doi.org/10.1002/jqs.1010

Waliser, D. E., & Graham, N. E. (1993). Convective cloud systems and warm-pool sea surface temperatures: Coupled interactions and self-regulation. *Journal of Geophysical Research*, *98*(D7), 12,881–12,893. https://doi.org/10.1029/93JD00872

Wara, M. W., Ravelo, A. C., & Delaney, M. L. (2005). Permanent El Niño-like conditions during the Pliocene warm period. *Science*, *309*(5735), 758–761. https://doi.org/10.1126/science.1112596

Xu, J., Holbourn, A., Kuhnt, W., Jian, Z., & Kawamura, H. (2008). Changes in the thermocline structure of the Indonesian outflow during Terminations I and II. *Earth and Planetary Science Letters*, *273*(1-2), 152–162. https://doi.org/10.1016/j.epsl.2008.06.029

<u>Supplementary material to *Geophysical Research Letters* manuscript 2019GL083035</u>

"A 5.3-million-year history of monsoonal precipitation in northwestern Australia"

Jan-Berend W. Stuut[1,2,3,*], Patrick De Deckker[4], Mariem Saavedra-Pellitero[5,#], Franck Bassinot[6], Anna Joy Drury[2], Maureen H. Walczak[4], Kana Nagashima[7], Masafumi Murayama[8]

[1]NIOZ – Royal Netherlands Institute for Sea Research, and Utrecht University, Texel, the Netherlands
[2]MARUM – Center for Marine Environmental Sciences, Bremen University, Bremen, Germany
[3]Department of Earth Sciences, Faculty of Science, Vrije Universiteit Amsterdam, The Netherlands
[4]Australian National University, Research School of Earth Sciences, Canberra, Australia
[5]Bremen University, Department of Geosciences, Bremen, Germany
[6]LSCE - Laboratoire des Sciences du Climate et de l'Environnement (CEA, CNRS, UVSQ), Gif-sur-Yvette, France
[7]Research Institute for Global Change, Japan Agency for Marine-Earth Science and Technology-JAMSTEC, Yokosuka, Japan
[8]Center for Advanced Marine Core Research, Kochi University, Kochi, Japan
[#]now at: School of Geography, Earth and Environmental Sciences, University of Birmingham, UK
[*]corresponding author: jb.stuut@vu.nl

Selection of core sites

The detailed bathymetric map depicted in Figure S1 shows the exact core locations of the two studied cores ODP122-762B and MD002316. These core sites were selected on the basis of bathymetric mapping and seismic profiling carried out in 1988 and 2000, respectively. The core sites were chosen such that they are not prone to contain the results of mass wasting such as slope failure or turbidite deposits. Core ODP122-762B was drilled on the top of the Montebello Saddle, which forms a large plateau on the northwestern Australian continental slope [*Haq et al.*, 1990]. Core MD002361 was retrieved from a saddle in between the Cape Range Canyon and the Cloates Canyon, to avoid mass deposits that may have flown through these canyons [*Spooner et al.*, 2011].

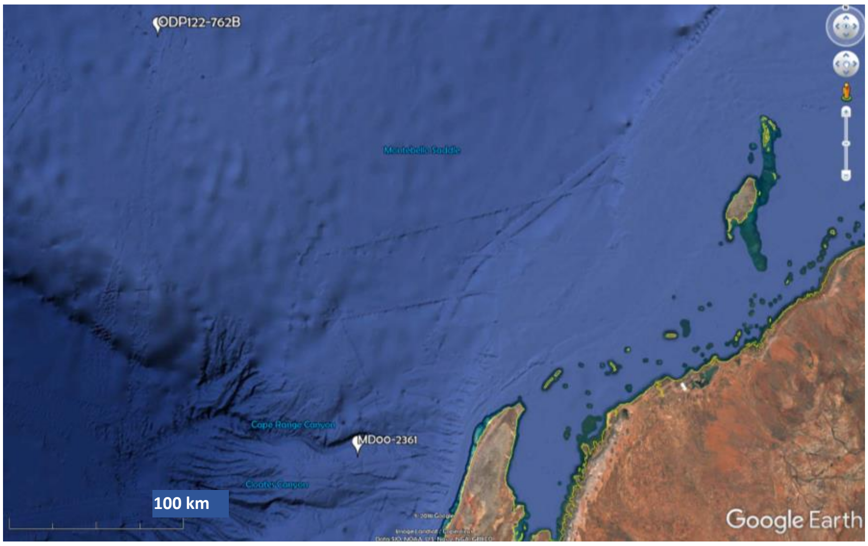

Figure S1. Detailed bathymetric map of the northwestern Australian continental slope with the exact positions of the core sites ODP122-762B and MD00-2361. Straight lines on the map show locations of detailed bathymetric mapping.

The two sediment cores were checked carefully for any signs of mass wasting which had not been found by Stuut et al., [2014] in the upper half of the core (<550 ka). A disturbance was found half way down core MD002361 at about 20m, and which was dated at about 1 Ma. This timing coincides with a large mass-wasting event that is well-known in the area and which was observed in numerous sediment records (Dr S. Gallagher, *pers. com*.). For this reason, we did not present the part of sediment core MD002361 older than 1 Myr. For sediment core ODP122-762B, no turbidite sequence has been observed by the sedimentologists on board *RV Joides Resolution [Haq et al., 1990]*, nor by us, nor in the papers by Tang [1992], nor in Wells and Chivas [1994]. The absence of this event in core ODP122-762B at about 1 Myr most likely is related to the fact that also this core was drilled from a ridge that stands above channels through which a turbidite was most likely funnelled into the Indian Ocean or it is simply too distal for this event to have reached it. Further confirmation for continuous sedimentation stems from the uninterrupted $\delta^{18}O$ chronologies of both cores as well as the excellent correspondence in the bulk-chemical records between them.

Relationship between present-day precipitation and ENSO

Presently, the monsoonal climate of northern Australia is strongly influenced by the El Niño Southern Oscillation (ENSO), which is related to the Southern Oscillation Index (SOI). The SOI is a standardized index based on the observed sea-level pressure differences between the central-Pacific island of Tahiti and Darwin, Australia. These pressure differences reflect the east-west sea-surface temperature and air-pressure gradients typical for El Niño and La Niña episodes. A negative phase of the SOI represents below-average air pressure at Tahiti and above-average air pressure at Darwin. Prolonged periods of negative SOI values coincide with anomalously warm ocean waters across the eastern tropical Pacific, which are typical of El Niño episodes. The opposite holds for La Niña situations.

Typically, tropical-cyclone (TC) activity is increased during so-called neutral years and La Niña years [*Dare*, 2013]. Present-day observations confirm this relationship between the SOI, TC-related rainfall in northern West Australia, and river runoff [*Dare et al.*, 2012]. This relationship is illustrated by comparing the SOI with precipitation in the TC months (November – March) at three monitoring stations at airports in northwestern Australia and river runoff of three rivers draining into the eastern Indian Ocean: the Gascoyne River, Lyndon River and Ashburton River (figs.S2A and S2D). The general relationship is that during periods of positive SOI, rainfall and river runoff are increased. Rivers in northwestern Australia remain dry during most of the year and carry vast loads of suspended sediments during sparse flooding events (see fig.S2B: Gascoyne River at Nine-mile bridge during flooding event in 2010 and fig.S2C: the Gascoyne River spilling huge amounts of sediments into the eastern Indian Ocean during the flooding event following TC Kelvin in March 2018). These large amounts of sediments are eventually deposited on the ocean floor of the northwestern Australian continental margin via the shallow Ningaloo *(counter)* Current (fig.1) and can be reconstructed on the basis of bulk chemistry and particle size of the terrigenous fraction. As a result, we interpret the observed changes in sediment composition in the two studied sediment cores in terms of fluvial-mud transport, ultimately related to monsoonal rainfall in northwestern Australia.

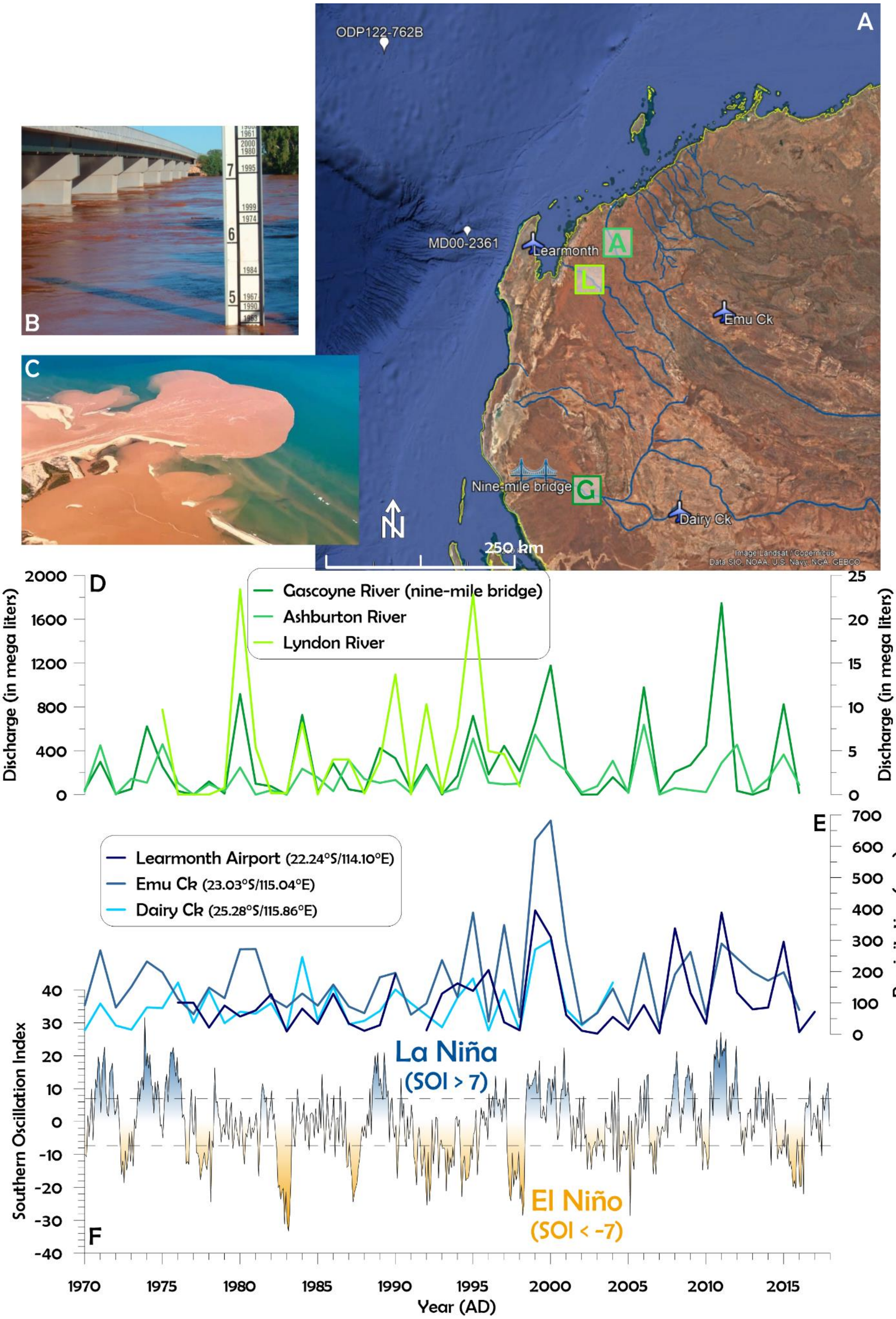

Figure S2. (A) Map of the study area indicating the core locations and airports in northwestern Australia where rainfall is being recorded as well the major rivers of which discharges have been plotted in figure D: G = Gascoyne River, recorded at nine-mile bridge, A = Ashburton River, L = Lyndon River. (B) photo of the Gascoyne River at nine-mile bridge during a flooding event in 2010 (from: <u>*double-*</u>

barreledtravel.com/the-gascoyne-river-comes-to-life) (C) the sediment load of the Gascoyne River spilling into the eastern Indian Ocean at Carnarvon after Tropical Cyclone Kevin in March 2018 (picture by Ryan John, from: www.perthnow.com.au/news/regional/was-gascoyne-river-flows-again-after-record-rain-ng-b887181z) (D) Discharge of three rivers draining into the study area: Lyndon River (much lower discharge, plotted on right y-axis, data until 1999), the Ashburton River, and the Gascoyne River measured at nine-mile bridge (E) TC-season (November – March) rainfall records recorded at the airports of Learmonth, Emu Creek and Dairy Creek, and (F), SOI. Data for records in D,E, and F were downloaded from the Australian Bureau of Meteorology website: www.bom.gov.au.

Dispersal of fluvial sediments in the deep sea

Although the distal core ODP122-762B is located on the northwestern continental shelf of Western Australia, about 330 km from the nearest coast, we claim that it directly registers the supply of fluvial sediments from rivers that drain the Western Australian hinterland. In a recent review of global sediment plumes by Shanmugam [2018], it was shown how suspended river sediments are dispersed both at the ocean's surface as well as along density layers of a large number of so-called hyperpycnal flows. In addition, just to name a few; River Nile floods were registered in the Mediterranean Sea at >200 km from the river mouth [*Ducassou et al.*, 2008], Congo River signatures were found in the Atlantic Ocean at >1000 km [*Hopkins et al.*, 2013; *Palma and Matano*, 2017], and Chinese river signatures were found in the South China Sea at >400 km from their estuary [*Kang et al.*, 2013]. In addition, the approach that we have taken is very similar to studies in the Indian Ocean [*Prins et al.*, 2000], in the southeast Atlantic Ocean [*Stuut et al.*, 2002], and in the southeast Pacific Ocean [*Stuut and Lamy*, 2004; *Stuut et al.*, 2007]. These studies all conclude that the proportion of fluvial mud increases with distance to the coast and that fluvial sediments are still clearly recognised up to 670 km from the river mouth, sedimentation rates are similar to the ones observed in our study.

Moreover, it was shown in sediment cores located at large distances from the Australian mainland (up to 600 km, see fig.S3-D) that alternating fluvial and aeolian sedimentation can be clearly distinguished during the past 25kyr on the basis of the same XRF-scanning technique that we apply [*Kuhnt et al.*, 2015]. These cores are located at large distances (up to 600 km, see fig.S3-D) from the Australian mainland.

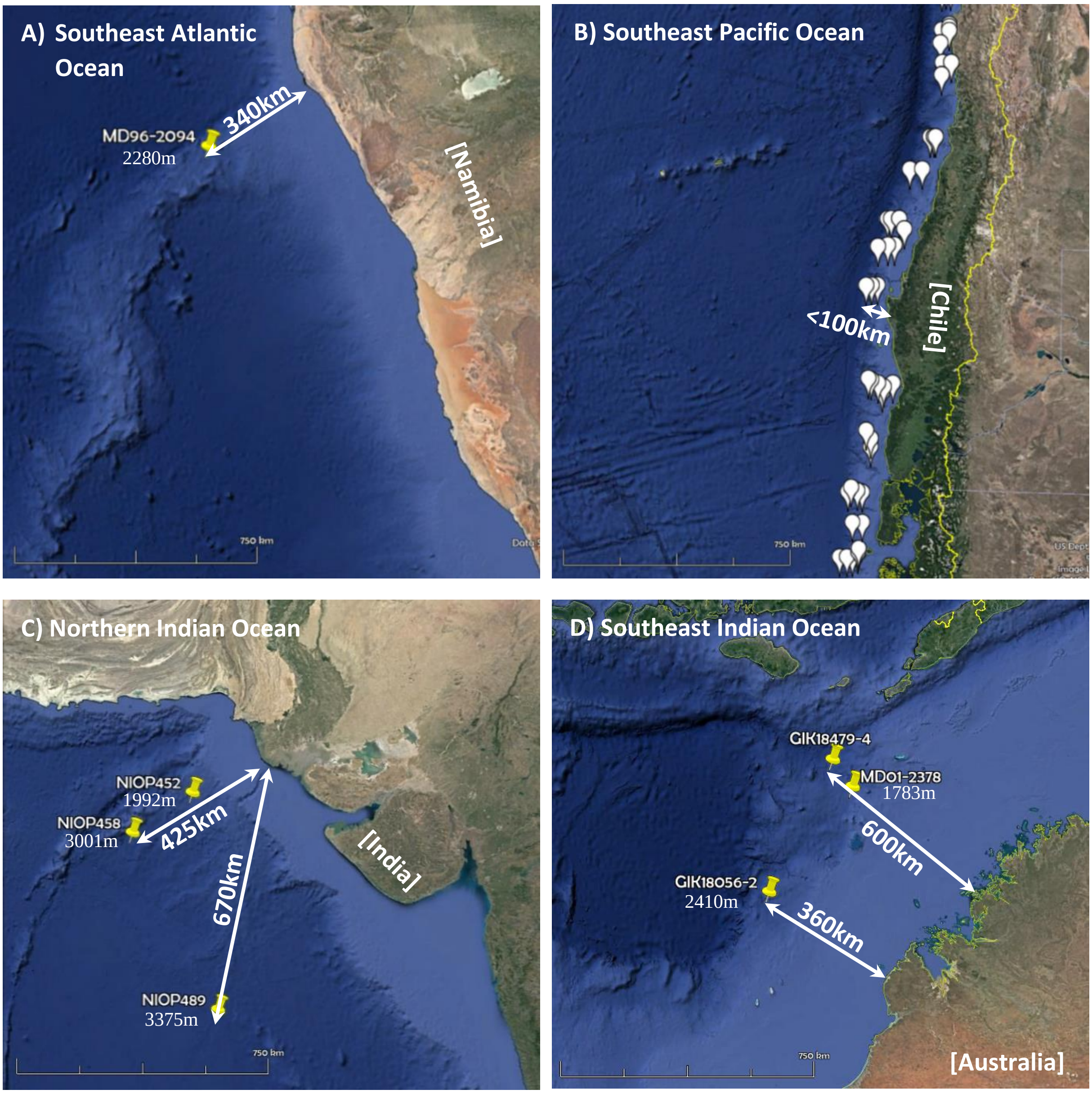

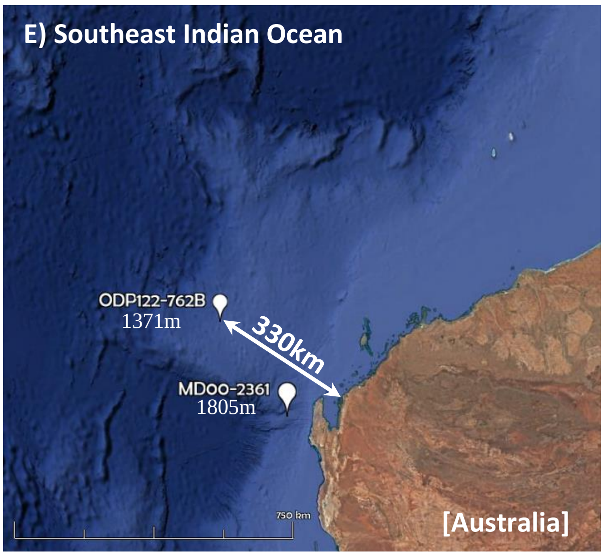

Figure S3. Google Earth maps of the core sites of four studies (*A [Stuut et al., 2002], B [Stuut and Lamy, 2004; Stuut et al., 2007], C [Prins et al., 2000], D [Kuhnt et al., 2015]*) compared with the Australian study area discussed in this paper (E). All studies distinguish between fluvial and aeolian sediments, recognising that the proportion fluvial sediments increases relative to aeolian with distance to the coast. The scale bar in each panel is 750 km. Arrows in figures A and B show distance to the nearest shore, which is actually much smaller than the actual distance to the river mouth.

.

Proxy records from bulk chemistry (XRF) and particle size

The combined evaluation of the bulk chemical analyses and particle size of the terrigenous fraction, published by Stuut et al., [2014] shows how the sediments of the upper part (last 500 ka) of sediment core MD00-2361 consist primarily of fluvial mud and wind-blown dust. The most evident proxies presented by Stuut et al., [2014] are summarised here (fig S4) and these results were extended for the MD00-2361 core down to 1 Ma in this paper.

Core MD00-2361 has a total length of 42m, of which the upper 22m cover the last 1 Ma (based on oxygen-isotope stratigraphy). At 23m core depth signs of mass wasting were observed, which may be related to a large turbidite that was found in many cores in the region at ~1 Ma (pers. Comm. Prof. S. Gallagher).

The two bulk-chemical proxies measured using an XRF core scanner (Log(Si/Al) and Log(Zr/Fe), see fig.S4) show how glacial- and interglacial stages are markedly different in sediment composition. Glacial stages are characterised by high Si and Zr values, which we interpret as typical aeolian origin. The interglacial stages are characterised by high Al and Fe values, which we interpret as typical fluvial origin. Based on an end-member approach applied to particle-size distributions of the terrigenous sediment fraction, Stuut et al., [2014] showed how at this proximal core site, the aeolian sediment fraction is distinctly coarser grained than the fluvial sediment fraction. Thus, for each sample the proportion aeolian dust and fluvial mud could be expressed, and which was interpreted as a proxy for continental humidity. The resulting downcore humidity record corroborates the bulk chemical records with a clear dominance of fluvial sediments during interglacial stages, as opposed to a dominance of aeolian sediments during glacial stages (fig. S5).

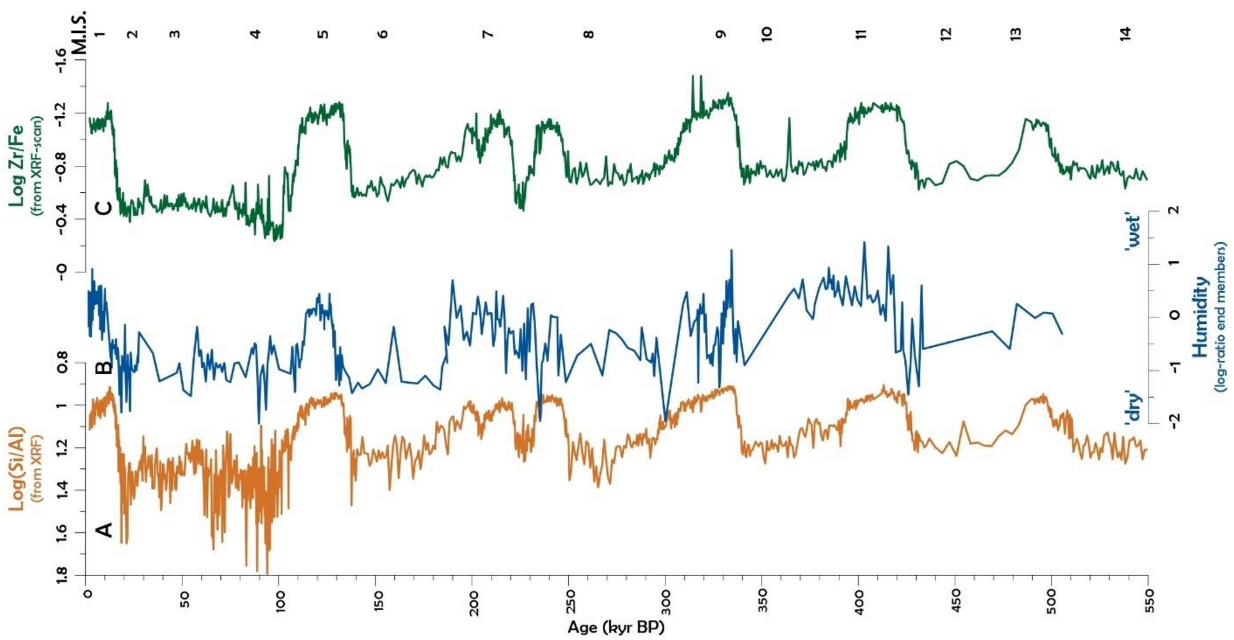

Figure S4. Most evident proxy records for northwestern Australian climate of the last 550 Ka (from core MD00-2361 and previously published by Stuut et al., [2014]. A) Log Si/Al, a proxy for different types of terrigenous sediment supply in which the Si is predominantly present in wind-blown dust as opposed to Al which is in the fine-grained fluvial mud; B) Continental humidity, expressed as a log-ratio of the fluvial and aeolian end members in the particle-size distributions of the terrigenous sediment fraction; C) Log Zr/Fe, a proxy for continental humidity with the Zr in the wind-blown sediment fraction and the Fe in the fluvial mud. MIS: Marine Isotopic Stages.

Linear sedimentation rates

Supporting evidence for the interpretation of our bulk-chemical and particle-size data follows from the linear sedimentation rates calculated by interpolating the amounts of sediment deposited per thousand years between the tie points of the age models of the two cores. Interglacial stages, which are dominated by fluvial sediments, ultimately related to intensive monsoonal activity, clearly show a pronounced higher amount of sediments deposited at the two sites as opposed to glacial stages, which consist mostly of marine carbonates and wind-blown coarse-grained quartz.

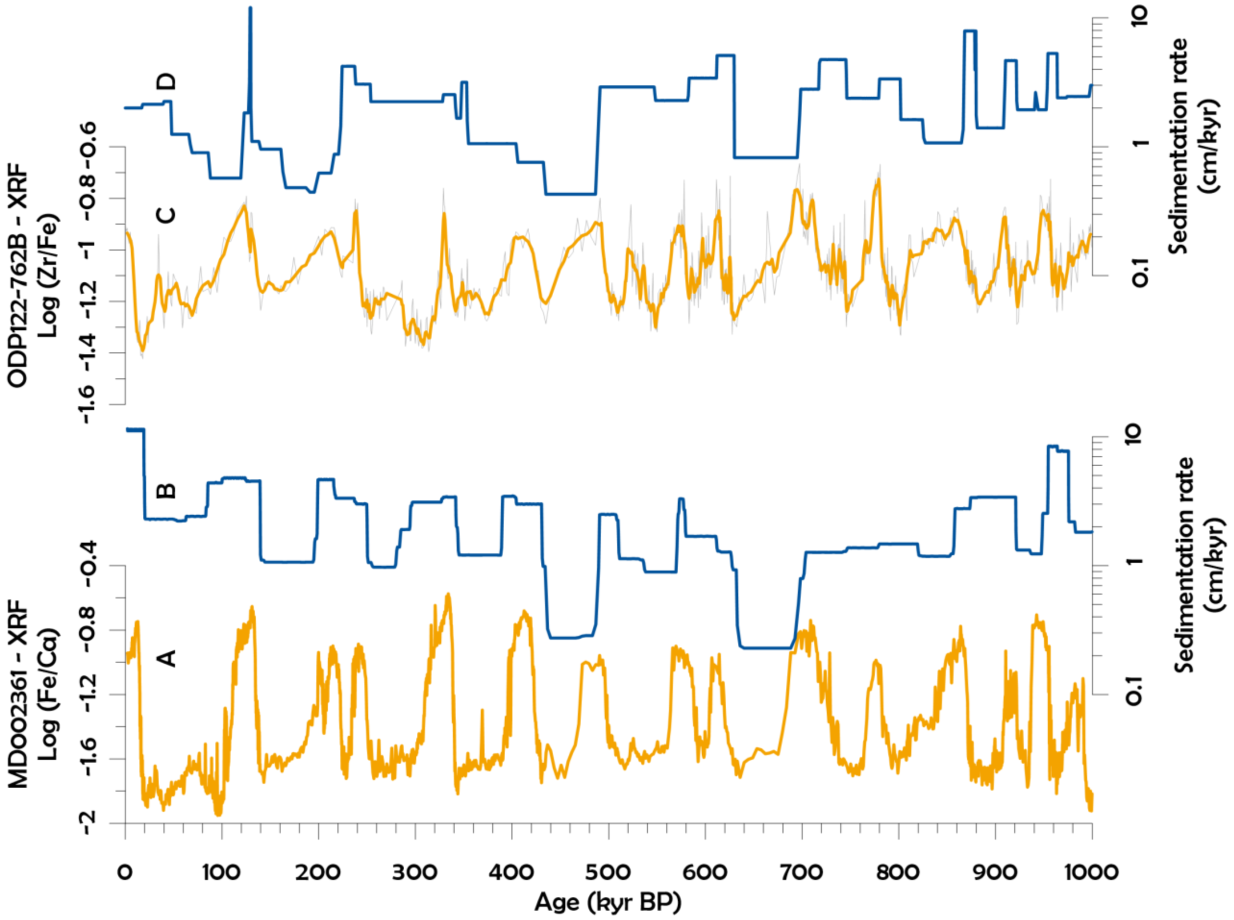

Figure S5. Proxy records for northwestern Australian climate of the last 1 Ma. A) MD00-2361 Log Fe/Ca, a proxy for terrigenous-sediment input [Stuut et al., 2014]. The lower 450 ka of the MD00-2361 records are new data, complementary to Stuut et al., [2014] B) MD00-2361 linear sedimentation rates as calculated from the age model showing high sedimentation rates during interglacial stages relative to glacial stages; C) ODP122-762B Log Fe/Ca raw data in grey, 5-point running average in orange; D) ODP122-762B linear sedimentation rates as calculated from the age model showing generally higher sedimentation rates during interglacial stages relative to glacial ones.

Measurements of bulk chemistry using XRF scans

Two different analysis types were used to obtain bulk-chemical records. The XRF records of core ODP122-762B were obtained using the Itrax XRF core scanner at Kochi Core Center, Japan. Elemental compositions of the elements Mg, Al, Si, P, S, Cl, Ar, K, Ca, Sc, Ti, V, Cr, Mn, Fe, Co, Ni, Cu, Zn, Ga, Br, Rb, Sr, Y, Zr, Ba, Ta, W, Os, Ir, Pt, and Pb were measured as counts per second. Due to the condition of the core sections, which were recovered from the ocean floor in 1988, only the heavier elements K to Zr gave reproducible measurements. Bulk chemical measurements of core MD002361 were obtained using the Avaatech XRF core scanner at NIOZ, the Netherlands. Elemental compositions of the elements Al, Si, S, Cl, K, Ca, Ti, Cr, Mn, Fe, Ni, Cu, Zn, Br, Rb, Sr, Y, Zr, and Pb were measured as counts per second. To avoid the problem of closed-sum [*Weltje and Tjallingii*, 2008], only Log-ratios of elements were used of Fe and Ca, representative of terrigenous and marine sediments, respectively. The Log(Fe/Ca) is therefore used as a proxy for land-derived material (see also the brown-coloured suspended sediments in the Gascoyne River in figs.S2B and S2C), in this case dominated by fluvial sediments supplied by the suite of rivers draining northwestern West Australia (fig.S2A).

In addition, zooming in on the terrigenous sediment fraction, we interpret the Log(Zr/Fe) as a proxy for wind-blown dust, also following Stuut et al., [2014]. In addition to these two proxies, we also investigated the Log(Si/Al) as a proxy for aeolian dust, knowing that the wind-blown material is dominated by quartz and the river-flown material is fine-grained and rich in aluminium [*Stuut et al.*, 2014]. To test the hypothesis that the aeolian and fluvial end members have distinctly different chemical compositions, we sampled dune systems and river beds in northwestern Western Australia (figs.1 and S6) and measured their bulk chemical composition using the Avaatech XRF scanner at NIOZ, using the same settings at which core MD00-2361 was measured.

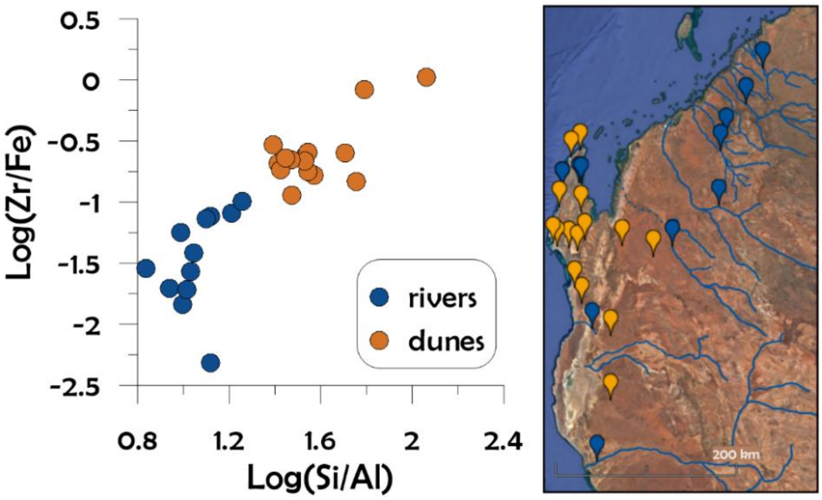

Figure S6. Bulk chemical composition of discrete samples from river beds and dune sediments in northwestern Western Australia. Cross plot of Log(Zr/Fe) and Log(Si/Al) shows how the two different types of sediment make up end-member compositions. These same bulk chemical ratios were plotted for the sediment core MD00-2361 in fig.S4, which further corroborate our interpretation of the proxy records.

The results show a distinct grouping of samples and a clear separation between the river samples and the dune samples with higher values for both Log(Si/Al) and Log(Zr/Fe) for the dune samples as opposed to the river samples. This separation into fluvial and aeolian end-members corroborates the bulk-chemical downcore results which show the same end-member separation throughout the last 1Ma (fig.S4). In addition, the data support the end-member approach based on the particle size with coarser-grained wind-blown sediments as opposed to finer-grained fluvial sediments.

Age model core ODP122-762B

The age model was based originally on the existing shipboard Magnetostratigraphy [*Tang*, 1992]. However, new calcareous nannofossil datum events [*Anthonissen and Ogg*, 2012], resulted in 16 new tie points (Table S1), which were assumed to be more precise than the preliminary shipboard data. In total, thirty-one smear slides were prepared and analyzed for calcareous nannofossils, from 4 m to 101,75 m in the same Leica DMRM polarized light microscope at 1000x. The samples were taken every ca. 3 m. Therefore, there could be certain uncertainty in the biostratigraphic datums. Being conservative and assuming an average sedimentation rate of 1.88 cm/kyr for this sedimentary sequence (calculated from the ODP122-762B-tiepoints-L&R05 list) and our sampling interval of ca. 3 m, the maximum shift in ages would be of ca. 0.17Ma. However, the succession of calcareous nannofossil markers at ODP122-762B was clear and we are confident on the first and last occurrences observed and considered for this work.

Subsequently, a visual correlation of the Log(Fe/Ca) XRF record and the Lisiecki and Raymo [2005] stack was made, which resulted in 175 additional tie points (fig S7).

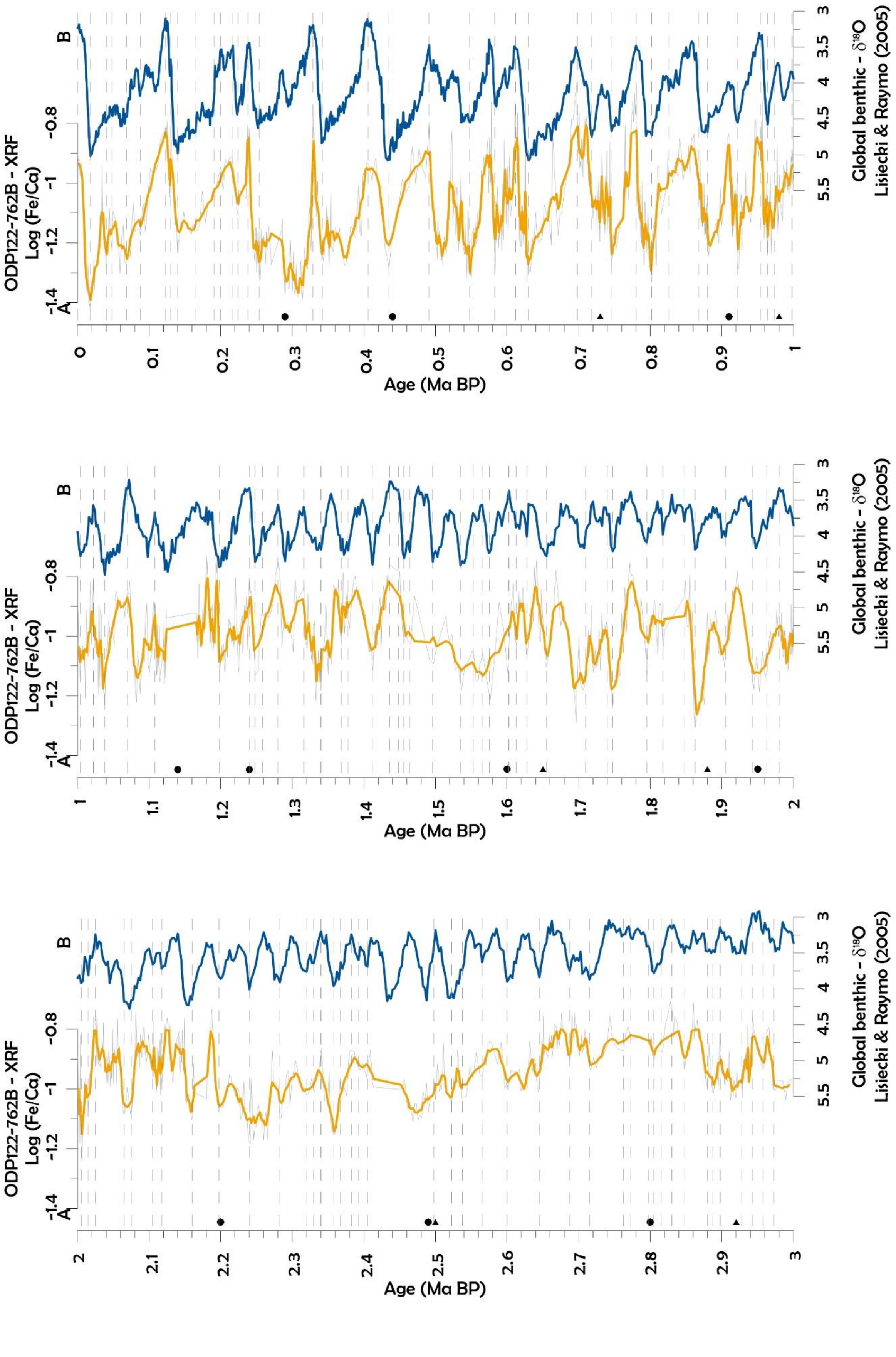

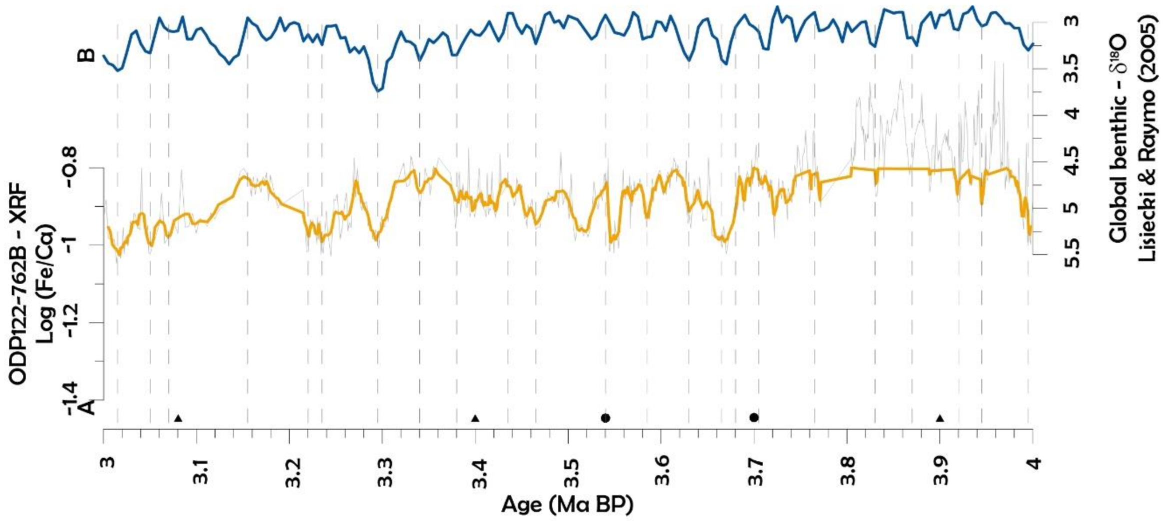

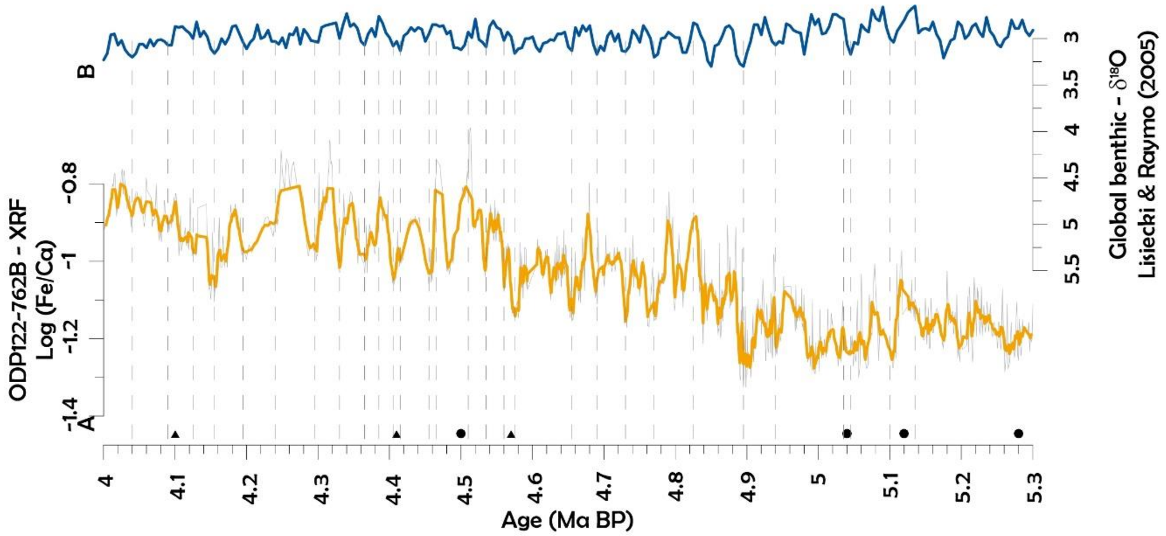

Figure S7. Plots showing the tie-points of the visual correlation of the Log(Fe/Ca) record to the Lisiecki & Raymo [2005] benthic stack. Also, the original magnetostratigraphic tie points by Tang [1992; black dots, N=16] and the new biostratigraphic tie points [black triangles, N=13] are shown.

Table S1. Biostratigraphic tie points obtained in this study based on calcareous nannofossil analyses compared with shipboard magnetostratigraphic tie points [Tang, 1992] on which the initial age model was based (FO: first occurrence, LO: last occurrence). Revised tie points of original shipboard Magnetostratigraphy are shown in grey.

Biostratigraphic Datum	Depth (mbsf)	Age (Ma)	Magnetostratigraphic Marker	Depth (mbsf)	Age (Ma)
FO *Emiliania huxleyi*	4	0.29	**Brunhes/Matuyama**	11.20	0.73
LO *Pseudoemiliania lacunosa*	7	0.44	**upper Jaramillo**	12.10	0.91
LO *Reticulofenestra asanoi* (common)	16.25	0.91	**lower Jaramillo**	13.10	0.98
FO *R. asanoi* (common)	22.75	1.14	**upper Olduvai**	25.00	1.65
LO Large *Gephyrocapsa* (>5.5 µm)	25.75	1.24	**lower Olduvai**	27.50	1.88
LO *Calcidiscus macintyrei*	29	1.6	**Matuyama/Gauss**	37.60	2.50
LO *Discaoaster triradiatus*	32.25	1.95	**Kaena**	47.20	2.92
FO *D. triradiatus* (acme)	38.5	2.2	**Mammoth**	51.40	3.08
LO *Discoaster surculus*	41.75	2.49	**Gauss/Gilbert**	62.10	3.40

LO *Discoaster tamalis*	44.75	2.8	**Cochiti**	71.60	3.90
LO *Sphenolithus* spp.	54.25	3.54	**Nunivak**	79.50	4.10
LO *Reticulofenestra pseudoumbilicus*	57.5	3.7	**Sidufjall**	84.50	4.41
LO *Amaurolithus primus*	73.25	4.5	**Thvera**	90.00	4.57
LO *Ceratolithus acutus*	89.25	5.04			
FO *Ceratolithus rugosus*	95.5	5.12			
LO *Triquetrorhabdulus rugosus*	101.25	5.28			

The samples were taken every ca. 3 m. Therefore, there could be certain uncertainty in the biostratigraphic datums. Being conservative and assuming an average sedimentation rate of 1.88 cm/kyr for this sedimentary sequence (calculated from the ODP122-762B-tiepoints-L&R05 list) and our sampling interval of ca. 3 m, the maximum shift in ages would be of ca. 0.17Ma. However, the succession of calcareous nannofossil markers at ODP122-762B was clear and we are confident on the first and last occurrences observed and considered for this work.

Time-series analysis

Power spectra were generated for the 5.3 Ma XRF records using the updated [*Grinsted et al.*, 2004] method of Torrence and Compo [1998], after detrending the data using a notch filter (removal of >1 Ma trend) and correcting for low-frequency wavelet bias following Liu et al., [2007]. In general, the detrended XRF wavelets show a stronger 40 ka beat at ~3 – 2.5 Ma and then a strong 95/125 Ka beat appearing just after 1 Ma, which is the well-known transition from the obliquity-dominated world to the eccentricity-dominated world at the mid-Pleistocene transition [*Lisiecki*, 2010; fig.S8].

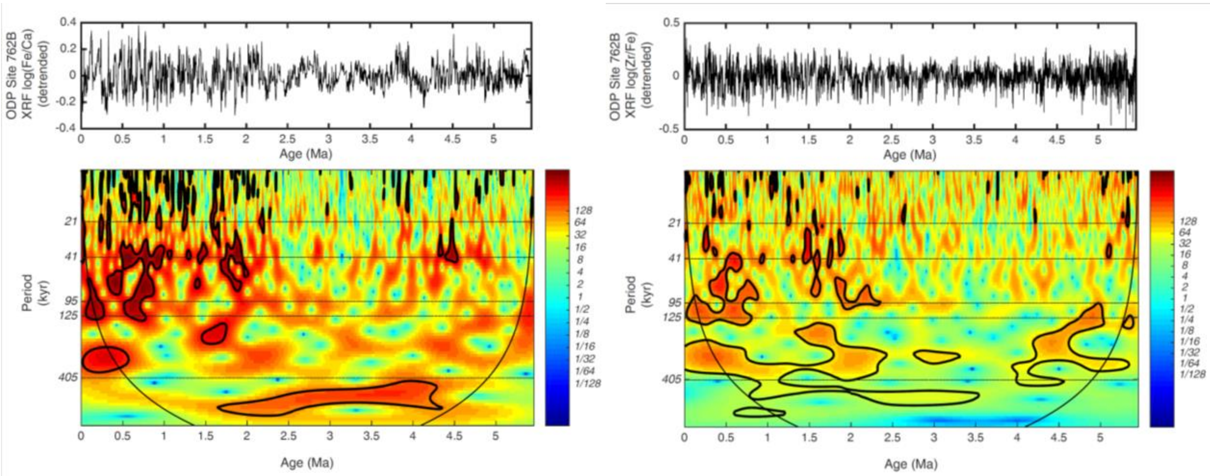

Figure S8. Power spectra of the XRF records Log(Fe/Ca) and Log(Zr/Fe for core ODP122-762B). See text above for more information.

Cited references

Anthonissen, D. E., and J. G. Ogg (2012), Appendix 3 - Cenozoic and Cretaceous Biochronology of Planktonic Foraminifera and Calcareous Nannofossils, in *The Geologic Time Scale*, edited, pp. 1083-1127, Elsevier, Boston.

Dare, R. A. (2013), Seasonal Tropical Cyclone Rain Volumes over Australia, *Journal of Climate*, *26*(16), 5958-5964.

Dare, R. A., N. E. Davidson, and J. L. McBride (2012), Tropical Cyclone Contribution to Rainfall over Australia, *Monthly Weather Review*, *140*(11), 3606-3619.

Ducassou, E., T. Mulder, S. Migeon, E. Gonthier, A. Murat, M. Revel, L. Capotondi, S. M. Bernasconi, J. Mascle, and S. Zaragosi (2008), Nile floods recorded in deep Mediterranean sediments, *Quaternary Research*, *70*(3), 382-391.

Grinsted, A., J. C. Moore, and S. Jevrejeva (2004), Application of the cross wavelet transform and wavelet coherence to geophysical time series, *Nonlinear Processes in Geophysics*, *11*, 561-566.

Haq, B. U., and ODP122 scientists (1990), Summary and highlights of Leg 122, *Affiliation (analytic): National Science Foundation, Marine Geology and Geophysics, Washington, DC*, *122*, 5.

Hopkins, J., M. Lucas, C. Dufau, M. Sutton, J. Stum, O. Lauret, and C. Channelliere (2013), Detection and variability of the Congo River plume from satellite derived sea surface temperature, salinity, ocean colour and sea level, *Remote Sensing of Environment*, *139*, 365-385.

Kang, Y., D. Pan, Y. Bai, X. He, X. Chen, C.-T. A. Chen, and D. Wang (2013), Areas of the global major river plumes, *Acta Oceanologica Sinica*, *32*(1), 79-88.

Kuhnt, W., A. Holbourn, J. Xu, B. Opdyke, P. De Deckker, U. Röhl, and M. Mudelsee (2015), Southern Hemisphere control on Australian monsoon variability during the late deglaciation and Holocene, *Nature Communications*, *6*, 5916.

Lisiecki, L. E. (2010), Links between eccentricity forcing and the 100,000-year glacial cycle, *Nature Geoscience*, *3*(5), 349-352.

Lisiecki, L. E., and M. E. Raymo (2005), A Pliocene-Pleistocene stack of 57 globally distributed benthic $\delta^{18}O$ records, *Paleoceanography*, *20*(1), PA1003.

Liu, Y., X. S. Liang, and R. H. Weisberg (2007), Rectification of the Bias in the Wavelet Power Spectrum, *Journal of Atmospheric and Oceanic Technology*, *24*(12), 2093-2102.

Palma, E. D., and R. P. Matano (2017), An idealized study of near equatorial river plumes, *Journal of Geophysical Research: Oceans*, *122*(5), 3599-3620.

Prins, M. A., G. Postma, J. Cleveringa, A. Cramp, and N. H. Kenyon (2000), Controls on terrigenous sediment supply to the Arabian Sea during the late Quaternary: the Indus Fan, *Marine Geology*, *169*, 327-349.

Shanmugam, G. (2018), A global satellite survey of density plumes at river mouths and at other environments: Plume configurations, external controls, and implications for deep-water sedimentation, *Petroleum Exploration and Development*, *45*(4), 640-661.

Spooner, M. I., P. De Deckker, T. T. Barrows, and L. K. Fifield (2011), The behaviour of the Leeuwin Current offshore NW Australia during the last five glacial-interglacial cycles, *Global and Planetary Change*, *75*(1), 119-132.

Stuut, J.-B. W., and F. Lamy (2004), Climate variability at the southern boundaries of the Namib (southwestern Africa) and Atacama (northern Chile) coastal deserts during the last 120,000 yr, *Quaternary Research*, *62*(3), 301-309.

Stuut, J.-B. W., F. Temmesfeld, and P. De Deckker (2014), A 550 kyr record of aeolian activity near North West Cape, Australia: inferences from grain-size distributions and bulk chemistry of SE Indian Ocean deep-sea sediments, *Quaternary Science Reviews*, *83*, 83-94.

Stuut, J.-B. W., S. Kasten, F. Lamy, and D. Hebbeln (2007), Sources and modes of terrigenous sediment input to the Chilean continental slope, *Quaternary International*, *161*, 67-76.

Stuut, J.-B. W., M. A. Prins, R. R. Schneider, G. J. Weltje, J. H. F. Jansen, and G. Postma (2002), A 300-kyr record of aridity and wind strength in southwestern Africa: inferences from grain-size distributions of sediments on Walvis Ridge, SE Atlantic, *Marine Geology*, *180*(1-4), 221-233.

Tang, C. (1992), Paleomagnetism of Cenozoic sediments in Holes 762B and 763A, central Exmouth Plateau, Northwest Australia., in *Proceedings of the Ocean Drilling Program, Scientific Results*, edited by U. Von Rad, B. U. Haq and et al, pp. 717-733, Ocean Drilling Program, College Station, TX.

Torrence, C., and G. P. Compo (1998), A Practical Guide to Wavelet Analysis, *Bulletin of the American Meteorological Society*, *79*(1), 61-78.

Wells, P. E., and A. R. Chivas (1994), Quaternary foraminiferal bio- and isotope stratigraphy of ODP Holes 122–760A and 122–762B, Exmouth and Wombat Plateaus, northwest Australia, *Australian Journal of Earth Sciences*, *41*(5), 455-462.

Weltje, G. J., and R. Tjallingii (2008), Calibration of XRF core scanners for quantitative geochemical logging of sediment cores: Theory and application, *Earth and Planetary Science Letters*, *274*(3–4), 423-438.